ORIGINAL SCIENTIFIC PAPER

CROATICA CHEMICA ACTA

Croat. Chem. Acta **2026**, *99*(1)
Published online: June 28, 2026
DOI: 10.5562/cca4256

HKD 1926

An Enantioselective High-Throughput Colorimetric Assay for Rapid Screening of Oxidoreductases Producing Chiral Amines or Alcohols

Vasilis Tseliou,[1] Kyriakos Tsatsis,[1,2] Francesco G. Mutti[1,*]

[1] Van 't Hoff Institute for Molecular Sciences, HIMS-Biocat, University of Amsterdam, Science Park 904, 1098 XH, Amsterdam, The Netherlands

[2] Present address: Department of Biotechnology and Biomedicine, The Technical University of Denmark, Søltofts Plads, Building 221, DK-2800 Kgs,. Lyngby, Denmark

* Corresponding author's e-mail address: f.mutti@uva.nl

RECEIVED: January 26, 2026 * REVISED: June 05, 2026 * ACCEPTED: June 09, 2026

PROCEEDING OF THE SOLUTIONS IN CHEMISTRY 2024, 11–15 NOVEMBER 2024, SVETI MARTIN NA MURI, CROATIA

Abstract: High-throughput screening of oxidoreductases for enantioselectivity remains a key challenge in enzyme engineering, as traditional screening formats commonly provide activity data but not stereochemical discrimination. Herein, we describe a stereoselective colorimetric platform in which a monoamine oxidase variant selectively oxidizes (*S*)-configured amines to imines, releasing stoichiometric hydrogen peroxide that is detected through a horseradish peroxidase–mediated color reaction. This enables rapid screening in aqueous microplate formats, with color development that can be monitored in real time by standard plate readers. Control experiments confirmed the absence of background signal from (*R*)-configured amines or lysate components, demonstrating the assay's high selectivity. The concept was further extended to other oxidoreductases by coupling enzymatic product oxidation to oxidase-mediated hydrogen peroxide formation and subsequent horseradish peroxidase–driven color development. Validation with engineered amine dehydrogenase (AmDH) and alcohol dehydrogenase (ADH) confirmed both sensitivity and enantioselectivity of the colorimetric assay, with visual results also validated by gas chromatography. This approach provides a scalable and versatile tool for accelerating the discovery and optimization of stereoselective biocatalysts.

Keywords: biocatalysis, high-throughput screening, colorimetric assay, enantioselectivity, amine dehydrogenase, monoamine oxidase, alcohol dehydrogenases, enzyme engineering.

INTRODUCTION

THE chemical industry is increasingly driven toward greener and more sustainable synthetic routes, with a strong emphasis on achieving high enantioselectivity while minimizing environmental impact.[1–3] In this context, biocatalysis has emerged as a powerful tool, providing environmentally friendly, atom-efficient, and highly chemo- and stereoselective routes to valuable building blocks including chiral amines and alcohols.[4,5] Over the past decade, several families of biocatalysts have been developed for amine synthesis, notably amine dehydrogenases (AmDHs)[6] and imine reductases/reductive aminases (IREDs/RedAms).[7] These enzymes have gained remarkable momentum, spurring extensive enzyme engineering campaigns aimed at enhancing their performance in asymmetric catalysis, with some of them now applied at industrial scale.[8–11] This progress has been fueled by major advances in enzyme engineering methodologies, including molecular biology, directed evolution, metagenomic mining and machine learning.[12] However, a key challenge in optimizing enzyme properties through enzyme engineering is the efficient screening of large libraries of mutated enzymes (i.e., variants) to identify beneficial mutations. This requires high-throughput screening (HTS) assays capable of detecting enzyme activity and linking phenotype to genotype, thereby ensuring that desired traits can be traced back to their genetic origins. Additionally, for the evolution of stereoselective enzymes, enantioselective HTS methods (*ee*-HTS) that can rapidly and reliably distinguish between enantiomers are highly sought—ideally without the need of any sophisticated

equipment. The limited availability of such *ee*–HTS methods represents a critical bottleneck that currently constrains the laboratory evolution of highly selective biocatalysts.[13]

However, a range of *ee*-HTS assays have been developed over the past two decades. Spectrophotometric and fluorescence-based methods, such as UV/Vis assays with chiral para-nitrophenyl esters,[14] the EMDee assay (enzymatic method for determining enantiomeric excess) which exploits ADH enantioselectivity,[15] and DNA microarray fluorescence assays[16], are simple and sensitive but generally rely on surrogate substrates, existing enzyme scaffolds with known enantioselectivity, or multi-step sample preparation, and often show limited precision (± 10 % ee). Analytical techniques including chiral GC[17] or HPLC[18] remain the gold standard for accuracy but are too slow and labor-intensive for large-scale screening. More advanced platforms such as MS–[19–21] and NMR–[22] based assays offer high accuracy (± 2–5 %) and reasonable throughput, yet they typically require isotope labeling, derivatization, or precise reaction timing, together with specialized and expensive instrumentation. Similarly, FTIR-based assays allow measurements directly in culture supernatants and achieve high throughput, but are limited to substrates with IR-active functional groups.[23] Capillary array electrophoresis (CAE) provides some of the fastest enantioselectivity determinations available (up to 30,000 samples/day), though applications so far remain largely confined to chiral amines.[24] Finally, circular dichroism (CD)-based assays combined with HPLC separation offer a practical alternative, but their reliance on product separation makes their use in high-throughput enzyme engineering campaigns impractical.[25] In addition, microdroplet-based high-throughput screening technologies enable ultrafast analysis of millions of individual biocatalytic reactions per day with minimal reagent consumption, but they require highly specialized microfluidic instrumentation and expert operation, limiting their accessibility for most laboratories.[26]

Therefore, a broadly applicable, inexpensive, and enantioselective HTS assay that can be performed in aqueous microplate systems without derivatization or sophisticated equipment remains elusive. Simple colorimetric assays are especially attractive for this purpose, as they provide immediate readouts by eye or by standard plate readers, require minimal sample preparation, and are inherently scalable. However, most colorimetric assays applied to amine synthesis do not resolve enantioselectivity. For instance, a widely used colorimetric assay is based on formazan, in which enzymatic NAD^+ reduction to NADH is coupled—through phenazine ethosulfate (PES) as a mediator—to the reduction of colorless INT (2-(4-iodophenyl)-3-(4-nitrophenyl)-5-phenyltetrazolium chloride hydrate) to yield a red formazan dye detectable at 495 nm (Figure 1a).[27] While useful for activity screening, this assay implies that variants catalytically competent in the reductive amination direction are equally active in the reverse (deamination) direction, often leading to false negatives. False positives can also arise from non-specific tetrazolium reduction. Recently, this principle was adapted for IREDs/RedAms in the "IREDy-to-go" assay, which couples oxidative deamination-driven NAD(P)H formation to INT reduction, successfully detecting enzyme activity across variant panels.[28] Nevertheless, as with earlier formazan assays, enantioselectivity remains unresolved. Another simple NAD^+ autofluorescence assay (Figure 1b), for example, monitors NAD^+ formation under strongly alkaline conditions (pH > 13),[29] but suffers from low signal-to-noise, instability at high pH, and long incubation times, limiting throughput and sensitivity. A modified two-wavelength approach (340 / 600 nm) improves normalization but remains restricted to deamination reactions and is prone to substrate interference.[29,30] Parallel to these developments, a high-sensitivity, fluorescence-based enzyme cascade assay for NAD(P)H-dependent oxidoreductases has been described, achieving orders-of-magnitude greater sensitivity than conventional methods by linking enzyme turnover to downstream fluorescent signals such as the release of umbelliferon (Figure 1c).[31] While powerful, this system requires multi-enzyme coupling and fluorescence infrastructure, and like other fluorescence and formazan assays, it provides activity information but not enantioselectivity. Beyond amine-focused screens, a broad toolkit of HTS assays exists across oxidoreductases that inform our design choices. For oxidases, assays that couple hydrogen peroxide production to horseradish peroxidase are widely used, typically employing chromogenic dyes such as 2,2'–azino–bis(3–ethylbenzothiazoline–6–sulfonic acid) (ABTS),[32] 3,3',5,5'–tetramethylbenzidine (TMB),[33] or ortho–dianisidine,[34] and are readily adapted to microtiter plate or solid-phase formats (Figure 1d). Recently, oxidase-coupled colorimetric screening systems for reductive aminases and related oxidoreductases have also been reported. In particular, the "RedAm Detect" platform couples aminase-catalyzed product formation to an amine oxidase–HRP reporter system, enabling rapid, high-throughput activity screening of RedAms, AmDHs, and AADHs.[35] While this approach enables quantitative monitoring of amine-production activity and facilitates large-scale library screening, it does not directly address stereoselectivity or enantiomeric discrimination. Oxygenase activity can be monitored by coupling product formation to a horseradish peroxidase–hydrogen peroxide system, in which the initial oxidation products are further converted into colored or fluorescent dimers and polymers (see Figure 1e for an example).[36] These strategies underscore the

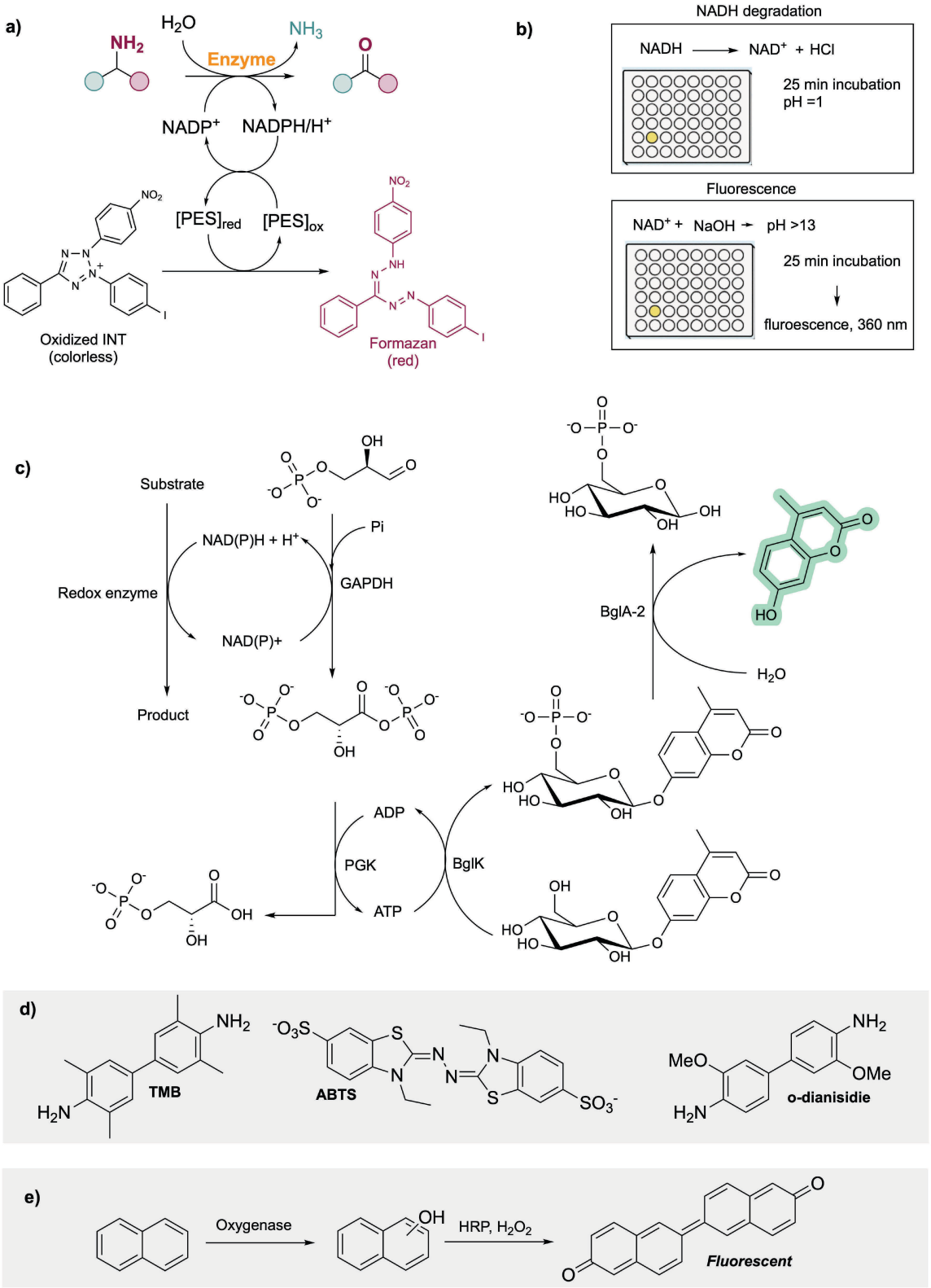

Figure 1. a) Example of application of formazan-based assay: NAD(P)H generated by the primary enzyme reduces tetrazolium salts to colored formazans. b) NAD^+ autofluorescence assay: NADH is acid-degraded and NAD^+ is converted into a fluorescent species under strongly alkaline conditions. c) High-sensitivity fluorescence cascade: enzyme-generated $NAD(P)^+$ is amplified

versatility and scalability of colorimetric reporting systems across oxidoreductases. However, they almost exclusively provide information on overall catalytic activity but not enantioselectivity, highlighting the central challenge that motivates the development of stereochemically discriminating, colorimetric high-throughput screening assays.

In this study, we report the development of a robust, *ee*-HTS assay for the detection of (*S*)-configured amines formed via reductive amination (Figure 3). The method is designed to directly evaluate the activity of potential (*S*)-selective AmDHs, including engineered D-AADH variants, in the synthetically relevant direction without requiring reverse (deamination) activity or artificial surrogate readouts. Instead, the assay relies on the stereochemistry of the amine product which is oxidized by an enantioselective monoamine oxidase enzyme[37] (MAO) to the corresponding imine, generating stoichiometric hydrogen peroxide (H_2O_2) as a byproduct. This H_2O_2 is then detected through a horseradish peroxidase–catalyzed colorimetric cascade, enabling sensitive and real-time signal generation in aqueous solutions without the need for extraction or derivatization. Crucially, no colorimetric signal is observed in the presence of (*R*)-configured amines or in the absence of the amine product, thereby eliminating false positives and ensuring high enantio-discrimination. By focusing on the product of interest in the synthetically relevant direction, this system addresses key limitations of previous AmDH screening assays and provides a direct and selective tool for the discovery and engineering of AmDHs for asymmetric synthesis.

METHODOLOGY

Electrocompetent Cells and Electroporation

For the preparation of electrocompetent cells, a glycerol stock of *E. coli* BL21(DE3) cells containing no plasmid, was used for streaking an antibiotic-free LB–agar plate, grown overnight at 37 °C. Next day, a single colony was used to inoculate an overnight culture (ONC) containing LB medium (5 mL). This ONC was used to inoculate the main culture (500 mL). When the OD was ~ 0.7–1, the main culture was chilled on ice for 20 min. After this time, the main culture was transferred under flame to 10 sterile falcon tubes (10 x 50 mL) on ice. The falcon tubes were centrifuged for 15 min at 4500 rpm (4000g). The supernatants were removed, and it was ensured that no supernatant remained in the falcon tubes that could affect the transformation efficiency. The harvested cells were gently resuspended under flame in 50 mL ice cold 10 % v v^{-1} glycerol (sterile) and the samples were centrifuged for another 15 min at 4500 rpm. The supernatants were removed, and the pellets were resuspended in another 25 mL of 10 % *v* / *v* ice cold glycerol. After another round of centrifugation (4500 rpm) and removal of the supernatants, the cells were finally resuspended in 2 mL 10 % *v* / *v* ice cold glycerol under sterile conditions. Aliquots of 40 µL were prepared and the electrocompetent cells were stored at –80 °C. For the electroporation, an aliquot of 40 µL of cells was used and gently mixed with 1.5 µL of the plasmid encoding for the D–AADH (pET28b). The mixture was cooled on ice for 1 min and transferred to a pre-cooled cuvette (sterile, 0.2 cm) under flame. The cuvette was inserted into the slide of the shocking chamber and a single pulse was delivered with the optimal voltage of 2.5 kV. The cuvette was removed from the chamber and 1 mL of SOC medium was immediately added. The cells were gently resuspended and transferred to a 17 × 100 mm polypropylene tube which was incubated for 1 h at 37 °C.

Development of an Expression and Purification Assay in 96-Deep Well Blocks

For the development of the high throughput screening method in 96-deep well blocks, modifications of the protocol reported by Bougioukou et al.[38] were made in order to optimize the process. The cFL1–AmDH was used as model enzyme because of its favorable properties. Aliquots of 100 µL ONC were used to inoculate new 96–deep well block containing 400 µL of LB medium (in the case of 1 mL 96–well plate) or 900 µL of LB medium (in the case of 2 mL 96–well plate), supplemented with 50 µg mL^{-1} kanamycin. After 3 h incubation at 37 °C with shaking at 390 rpm, another 500 µL (for the 1 mL blocks) or 1 mL (for the 2 mL blocks) of LB medium supplemented with 50 µg mL^{-1} kanamycin and 1 mM isopropyl-β-D-1-thiogalactopyranoside (IPTG) were added (final concentration of IPTG was 0.5 mM) and the plate was incubated at 25 °C overnight. The expression levels were observed by SDS-PAGE. The next day, the plate was centrifuged, and the supernatants were discarded. The pellets were frozen at –20 °C for at least one hour followed by thawing and resuspension in 150 µL washing buffer (potassium phosphate buffer pH 7.0, NaCl, Tween 20, 0.04 % NaN_3, IMAC purification kit). The plate was then shock-frozen in liquid nitrogen and immediately thawed with warm water for five times. The lysis of the cells was finally completed by the addition of lysozyme (2 mg mL^{-1}) for 2 h at 4 °C and shaking in an orbital shaker (390 rpm). After incubation, the lysate was centrifuged at 5600 rpm for 45 minutes and the supernatants were collected for purification.

Purification was performed with QuickPick IMAC kit protocol using PickPen 8–M, after modifications of manufacturer's instructions. Magnetic beads (100 µL) were transferred to 150 µL regeneration buffer (aqueous $NiSO_4$

solution, Tween 20, 0.02 % NaN_3) and washed with washing 1 buffer (potassium phosphate buffer pH 7.0, NaCl, Tween 20, 0.04 % NaN_3). After that, the beads were transferred to the sample (150 µL) and incubated at RT for 20 min with shaking at 700 rpm using an orbital shaker. After one washing step with washing 2 buffer (100 mM potassium phosphate buffer pH 7.0, 250 mM NaCl, Tween 20, 0.04 % NaN_3, 20 mM imidazole), the protein was eluted with 100 µL elution buffer (50 mM sodium phosphate buffer, 300 mM imidazole, 500 mM NaCl, pH 8.0). The elution buffer composition, particularly the imidazole concentration, was optimized based on comparative elution trials using purified cFL1-AmDH, evaluating 300 mM versus 500 mM imidazole and various elution volumes (50 µL, 70 µL, and 140 µL) to maximize protein recovery in a single step. Additionally, the incubation times for both the sample-bead binding step (2 × 20 min) and the elution step (1 × 10 min) were optimized through preliminary experiments to ensure efficient protein capture and recovery.

For the high-throughput biocatalytic reactions, the purified enzymes were used immediately without storage. A reaction premix was prepared containing 2 M $HCOONH_4$ / NH_3 buffer (pH 8.5), 2 mM NAD^+, formate dehydrogenase (FDH, 3 mg in 10 mL), and 10 mM of the substrate (4'–fluorophenylacetone) dissolved in DMSO. The premix (100 µL) was dispensed into each well of a microtiter plate, followed by the addition of 100 µL of freshly purified enzyme, resulting in a final reaction volume of 200 µL per well. Reactions were incubated at 30 °C. After 24 hours, the reactions were quenched by the addition of 100 µL of 10 M aqueous KOH. Product extraction was performed using 250 µL of dichloromethane (CH_2Cl_2), followed by centrifugation to separate the phases. The organic layer was dried over anhydrous magnesium sulfate and analyzed by gas chromatography (GC-FID). Conversions were determined using an Agilent GC system equipped with an Agilent J&W DB–1701 column (30 m × 320 µm × 0.25 µm). GC conditions: injector temperature 250 °C; constant pressure 6.9 psi; oven temperature program: 60 °C (hold 6.5 min), gradient to 100 °C at 20 °C min^{-1} (hold 5 min), then gradient to 280 °C at 20 °C min^{-1} (hold 1 min).

Small Scale Expression and Purification of D–AADH

For the expression of D-AADH in 96-deep well blocks (2 mL), an ONC was prepared (10 mL LB medium supplemented with 50 µg mL^{-1} kanamycin). For each well of the plate, 100 µL of this ONC were used to inoculate 900 µL of LB medium supplemented with 50 µg mL^{-1} of kanamycin. These main cultures were grown at 37 °C for 3 h. After this time, a 1 mL LB medium supplemented with 50 µg mL^{-1} kanamycin and 1 mM IPTG was added to each well and the cultures were grown at 25 °C overnight. The next day, the plate was centrifuged at 5600 rpm for 1 h. The supernatants were removed, and the pellets were resuspended in 150 µL lysis buffer (pH 8.0, 50 mM KH_2PO_4, 300 mM NaCl). In total 50 µL from a home-made cell lysis reagent [(900 µL B-PER bacterial protein extraction reagent, 96 µL lysozyme of 100 mg mL^{-1} (concentration of stock solution) and 4 µL DNase of 10 mg mL^{-1} (concentration of stock solution)] were added to each sample and incubated at 25 °C for 90 min to allow for enough time for cell disruption. The lysates were centrifuged for 90 min at 5700 rpm and the supernatants were transferred in a flat-bottom 96-well plate for downstream purification.

Purification was performed with 50 µL of beads using the following procedure. For each sample (well) to be purified, 50 µL of beads were transferred to a 96–well plate. This plate was put on top of a home-made magnetic plate to keep the beads on the bottom of the plate and the liquid phase (storage solution) could be easily removed. 250 µL of lysis buffer was added to the well containing the beads. The beads were incubated in lysis buffer for 1 min. After that, the lysis buffer was removed and 100 µL of regeneration buffer were added to the beads and incubated for another minute. After the incubation time, the regeneration buffer was removed and another 250 µL of lysis buffer were added to the beads. After another minute, the lysis buffer was removed following by the addition of the 200 µL lysate. The lysate was incubated with the Ni^{2+} magnetic beads for 10 min at 4 °C. After that time, the 96–well plate containing the beads was placed on the top of the magnetic plate and the liquid phase was removed. 250 µL of wash buffer (pH 8.0, 50 mM KH_2PO_4, 300 mM NaCl, 30 mM imidazole) were added and incubated for 2 min. Finally, the enzyme was eluted with 50 µL elution buffer (pH 8.0, 50 mM KH_2PO_4, 300 mM NaCl, 500 mM imidazole) after incubation of another 5 min. After this step, the elution buffer containing the enzyme was stored and the beads were incubated in 200 µL elution buffer to remove any traces of bound enzyme.

The enzyme concentration was determined using the Bradford assay. A BSA stock (10 mg mL^{-1}) was prepared. Using this stock, samples with different concentrations of BSA (0.15–0.5 mg mL^{-1}) were prepared. 20 µL of each sample were added in 980 µL of Bradford solution and the absorbance at 595 nm was determined. Based on the obtained values, a calibration curve was determined with slope 0.791 (R^2: 0.993). A diluted sample (1 : 2, *v* / *v*) of the purified D-AADH was prepared and 20 µL of this sample were added into 980 µL Bradford solution and the absorbance at 595 nm was measured. In

order to calculate the concentration of the enzyme (mg mL^{-1}), the obtained value was divided by the slope and multiplied by the dilution factor (2).

Expression of MAO-D5

E. coli BL21(DE3) cells (glycerol stocks) harboring pET-28a plasmids encoding for the MAO–D5 and MAO–D9 were used to prepare ONCs (5 mL LB medium supplemented with ampicillin 100 μg mL^{-1}). Next day, 100 μL of the ONCs were used to inoculate 10 mL of LB medium supplemented with ampicillin 100 μg mL^{-1}. This small main culture was grown at 30 °C until the OD_{600} ~ 0.7–1 was reached. After the required time, 8 mL of this culture was used to inoculate the main large culture (800 mL of LB medium supplemented with ampicillin 100 μg mL^{-1}), which was grown at 30 °C overnight. The next day, the cells were harvested by centrifugation (15 min, 4500 rpm at 4 °C) and the pellet was resuspended in 50 mM KPi buffer, pH 7.6. Lysis of the cells was performed with ultrasonication (total sonication time 10 min). After centrifugation, the soluble part was stored at –80 °C supplemented with FAD and used as cell free extract in all reactions performed.

Colorimetric Assays for the Detection of (*S*)-configured Amines

2,4,6-TRIBROMO-3-HYDROXYBENZOIC ACID-BASED ASSAY

In this assay, 15 μL of the supernatant (cell free extract) containing MAO-D5 supplemented with FAD was used. Using 0.75 mM of 4–aminoantipyrine (AAP, compound 2, 1 M stock in DMSO) and 0.54 mM of 2,4,6-tribromo-3-hydroxybenzoic acid (compound 1, stock 2 % *w* / *v* in DMSO), an assay solution was prepared in 100 mM KPi, pH 7.6. The reaction consisted of 180 μL of assay solution, 15 μL of MAO-D5 cell free extract and 5 μL of horseradish peroxidase (HRP) solution (HRP stock 1 mg mL^{-1}). The reaction was started by the addition of amine (stock 1 M) at the desirable concentration.

CHROMOTROPIC ACID BASED ASSAY

AAP (compound 2) and 500 mM of chromotropic acid (CTA, compound 4) were prepared as stock solutions in DMSO. In addition, 1 M H_2O_2 stock solution in dH_2O was freshly prepared. The assay solution 2 (1 mL) was prepared by adding 3 mM AAP, 15 mM CTA and 10 mM H_2O_2 in either 100 mM sodium phosphate buffer pH 6.5 or 100 mM KPi buffer, pH 7.6. The substrate (5 mM) was added from a stock solution 1 M in DMSO. Reaction was started by the addition of 10 μg mL^{-1} HRP. Reactions were measured spectrophotometrically using a fluorometer with excitation filter A-590 and without any emission filter.

EXPRESSION AND PURIFICATION OF Lb-ADH AND YcnD

Lb-ADH was expressed and purified as reported in our previous study.[39]

E. coli BL21(DE3) cells transformed with plasmid encoding YcnD were streaked on LB agar plates containing ampicillin (100 μg mL^{-1}) and incubated overnight at 37 °C. Single colonies were used to inoculate 150 mL LB cultures, which were grown overnight at 30 °C with shaking. The next day, these pre-cultures were used to inoculate 800 mL main cultures supplemented with 100 μg mL^{-1} ampicillin. Cultures were grown at 30 °C until OD_{600} reached 0.6–1.0, at which point protein expression was induced with 0.5 mM IPTG and continued overnight at 30 °C (115 rpm). Cells were harvested by centrifugation (4,500 g, 15 min, 4 °C), washed with ice-cold 100 mM Tris-HCl buffer (pH 8.0), and stored at –20 °C. For lysis, cell pellets were resuspended in His-lysis buffer (50 mM sodium phosphate, 10 mM imidazole, 10 mM NaCl, pH 8.0) and supplemented with a trace of FMN when required. Sonication was performed for 5–10 min (amplitude: 45 %, 5 s ON / 5 s OFF pulses), followed by centrifugation at 18000 rpm for 50 min at 4 °C. Soluble and insoluble fractions were analyzed by SDS-PAGE. Soluble supernatants were filtered (0.45 μm) and purified via Ni-NTA affinity chromatography using pre-packed HisTrap FF columns (GE Healthcare). Columns were equilibrated with 10 column volumes (CV) of lysis buffer, followed by sample loading. Unbound proteins were washed with 10 CV of lysis buffer and 5 CV of wash buffer (50 mM sodium phosphate, 25 mM imidazole, 300 mM NaCl, pH 8.0). Target proteins were eluted with elution buffer (50 mM sodium phosphate, 300 mM imidazole, 300 mM NaCl, pH 8.0). Protein concentrations were determined spectrophotometrically using the flavin absorbance at 449 nm and standard equations ($C = A / \varepsilon d$). Protein purity was assessed by SDS-PAGE, and purified enzymes were stored in dialysis buffer until use.

RESULTS

Expression and Purification in 96–well Plates

An AmDH, namely the cFL1-AmDH (also abbreviated as Ch1-AmDH),[40,41] was selected for assay development due to its high expression levels, minimizing the risk of false negatives caused by poor enzyme yield. Cultivation trials were carried out in 1 mL and 2 mL volumes in 96-deep-well blocks to identify optimal growth conditions. In both formats, robust expression was achieved, with 2 mL cultures providing higher yields. Cell lysis under the optimized protocol produced sufficient soluble protein for downstream processing.

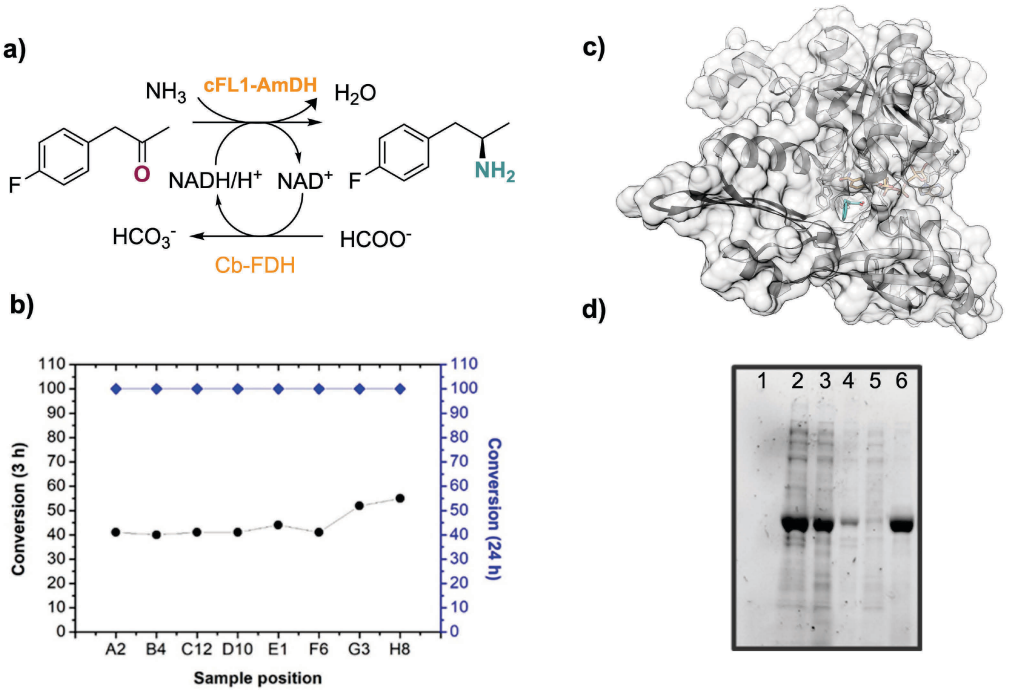

Figure 2. a) General scheme of biocatalytic reactions performed with amine dehydrogenases (AmDHs). b) Conversion of substrate *para*-fluoro phenylacetone to its corresponding amine product using cFL1-AmDH after expression and purification in 96-deep-well blocks; conversions were measured after 3 h (black line) and 24 h (blue line). c) Structural model of the D-AADH scaffold bound to phenylpyruvic acid generated with AlphaFold3. d) Expression and purification of D-AADH in 96-well plate format.

Purification was performed using Ni-NTA magnetic beads, with conditions optimized based on small-scale trials using known concentrations of cFL1-AmDH. Key parameters including bead binding capacity, incubation and elution times, imidazole concentration, and elution volume were systematically tested. Optimal recovery (~300 µg, 6 mg mL^{-1}) was achieved with 500 mM imidazole in a single 50 µL elution after 20 min binding and 5 min elution. SDS–PAGE analysis confirmed high purity and consistent yields across wells in both 1 mL and 2 mL formats.

To evaluate the reproducibility of enzymatic activity, the biocatalytic reactions were performed using the purified cFL1-AmDH from different well positions. Para-fluoro phenylacetone (Figure 2a), a known substrate for cFL1-AmDH was used together with 90 µM of enzyme.[6] Reactions were monitored at 3 h and 24 h. After 3 h, approximately 40 % conversion was observed across all samples, while complete conversion was reached after 24 h (Figure 2b), confirming both the reliability of the assay and consistency of enzyme performance across the plate.

As a potential scaffold for the development of (*S*)–selective AmDHs compatible with our screening platform, we selected D-AADH from *Corynebacterium glutamicum*.[42] D-AADH has a natural stereoselectivity that aligns with the desired (*S*)–amine configuration. The engineered enzyme natively produces D-amino acids; by replacing polar residues that interact with the α-carboxylate with hydrophobic ones, ketones (e.g., methyl ketones) or aldehydes as substrates might be accommodated in a similar binding orientation, leading to formation of (*S*)-configured amines. To explore this possibility, we first examined whether the parental scaffold could be expressed and purified under the same high-throughput conditions established for cFL1-AmDH. High expression levels were confirmed (Figure 2d, sample 2) compared to the sample before induction (Figure 2d, sample 1); additionally, cell lysis with B-PER reagent supplemented with lysozyme and DNase yielded most of the enzyme in the soluble fraction (Figure 2d, sample 3). Purification via Ni-NTA magnetic beads was efficient, with nearly complete binding—as no enzyme was detected in the buffer after bead removal (Figure 2d, sample 5)—and complete elution in a single fraction (Figure 2d, sample 6), mirroring the consistency observed with cFL1-AmDH. Protein quantification with the Bradford assay established that the 50 µL elution sample contained approximately 0.5 mg mL^{-1} of enzyme, corresponding to a total of 25 µg per sample.

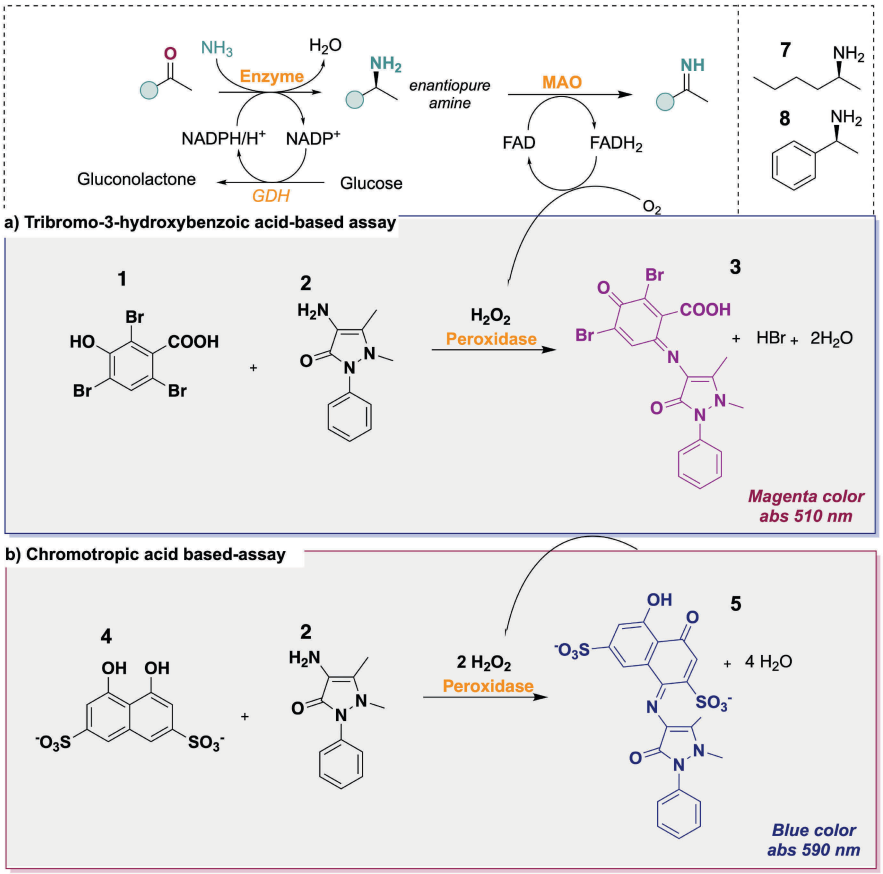

Figure 3. Investigated screening assays for enzyme variants using (a) 2,4,6-tribromo-3-hydroxybenzoic acid 1 or (b) chromotropic acid 4, respectively, with aminoantipyrine 2. For 3, the molar extinction coefficient (ε) at 510 nm is reported to be 2.9×10^4 M^{-1} cm^{-1} and remains constant under various assay conditions. In contrast, the molar extinction coefficient of 5 at 590 nm varies significantly depending on the assay conditions (e.g., 2.5–6.8×10^4 M^{-1} cm^{-1}). Since no generally accepted value has been established for chromophore 5 under our assay conditions, the molar extinction coefficient of 5 at 590 nm was calculated from the data in Table 2 and Figure 5 as 6.6×10^4 M^{-1} cm^{-1}.

These results confirmed that D-AADH from *Corynebacterium glutamicum* is compatible with the assay pipeline and justified its use as a suitable starting point for future mutagenesis aimed at generating a library of (*S*)-stereoselective AmDH variants. Such a mutagenesis campaign, however, requires the parallel development of a screening system capable not only of detecting amine formation but also of distinguishing the enantiomers.

Development of Enantioselective Colorimetric Assays

To this end, we sought a highly enantioselective enzyme that could selectively recognize one amine enantiomer and transform it into a product while yielding a colorimetric signal. Ideally, this transformation would be coupled to hydrogen peroxide generation, thereby linking enantiomer recognition directly to colorimetric detection. Colorimetric detection of hydrogen peroxide (H_2O_2) is a well-established strategy in biochemical assays, exploiting the ability of HRP to catalyze the oxidation of various substrates in the presence of H_2O_2, yielding a visible color change.[32–34] We therefore hypothesized that an enzyme capable of selectively oxidizing one enantiomer of an amine while releasing stoichiometric H_2O_2 would be an excellent candidate for such an assay. MAOs fulfill this role effectively, as they can selectively deaminate (*S*)-configured amines to their corresponding prochiral imines, with concurrent production of H_2O_2.[43]

To translate this into a robust readout system, we employed HRP in coupled colorimetric reactions (Figure 3) using either 2,4,6–tribromo–3–hydroxybenzoic acid (TBHBA, compound 1) or chromotropic acid (CTA, compound 4) in combination with 4-aminoantipyrine (AAP, compound 2). These substrates react in the presence of H_2O_2 to form intensely colored products such as compound 3 (magenta, λ_{max} = 510 nm) and compound 5 (blue, λ_{max} = 590 nm).

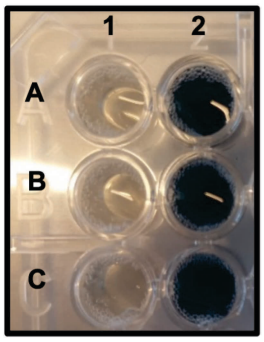

Figure 4. Initial validation of the colorimetric assay using the CTA/AAP-based system and (*S*)-2-heptylamine. Reaction wells A2–C2 contained 100 mM sodium phosphate buffer (pH 6.5), AAP (3 mM), CTA (15 mM), H_2O_2 (10 mM), (*S*)-2-heptylamine (5 mM), and HRP (10 μg mL^{-1}). Wells A1–C1 represented negative controls lacking HRP. The blue coloration observed in wells A2–C2 after 5 min confirmed HRP-dependent formation of the colored product, while the absence of color in wells A1–C1 confirmed the lack of non-enzymatic background signal under these conditions.

The resulting chromophores are readily detectable by eye or spectrophotometrically in high-throughput formats, enabling sensitive and selective monitoring of enantiomer formation. It is important to note that the primary objective of the developed assay is high-throughput qualitative screening for identifying enzyme variants producing the desired enantiomer. While the colorimetric signal correlates with the amount of oxidizable amine present, the system is not intended for precise quantification of enantiomeric excess, but rather for rapid hit identification and ranking of enantioselective variants at initial stages of evolution campaigns (hit / not hit).

To evaluate our hypothesis, we selected (*S*)–hexan–2–amine (7) and (*S*)–1–phenylethanamine (8) as model substrates (Figure 3). These amines are structurally similar to D-norleucine and D-phenylglycine, which can be synthesized by D-AADH, yet they lack carboxylic acid moiety. Importantly, both substrates have been reported to be accepted by the monoamine oxidase variant MAO-D5, making them suitable candidates for testing the enantioselective oxidation.[44] Moreover, their structural resemblance to the D-AADH products allows us to probe whether engineered variants could shift selectivity from carboxylated to non-carboxylated amine substrates in future work, and whether the resulting enantioselective conversion could be effectively detected through our H_2O_2-dependent colorimetric assay.

To evaluate the performance of the colorimetric assay, initial tests were conducted using 100 mM sodium phosphate buffer (pH 6.5), 3 mM AAP (compound 2), 15 mM chromotropic acid (CTA, compound 4), and 10 mM hydrogen peroxide. The reaction was initiated by the addition of HRP (10 μg mL^{-1}) and 5 mM of (S)-2-heptylamine (7). Within 5 minutes, a strong blue coloration was observed in the test reactions (Figure 4 wells A2–C2), while the negative control without HRP (NPC, non-protein control in wells A1–C1) remained colorless, confirming that the signal was enzyme-dependent.

To optimize conditions for MAO-D5, the reaction was also performed in 100 mM potassium phosphate buffer (KPi, pH 7.6), which is preferred by this enzyme. A similarly intense blue color developed after 5 minutes, and spectrophotometric measurements at 590 nm revealed higher absorbance values in KPi buffer compared to NaPi buffer. Importantly, negative control absorbance remained low (NPC < 0.25) after 30 minutes in KPi, indicating good signal-to-noise performance (Table 1).

Next, the assay's sensitivity to H_2O_2 was evaluated. Varying concentrations of externally added H_2O_2 (0–5 mM) were tested to determine the detection limit. As shown in Table 2, the assay reliably detected H_2O_2 concentrations as low as 0.1 mM, with the absorbance increasing in a concentration-dependent manner until saturation was observed at approximately 1 mM. The absorbance response was linear between 0 and 0.5 mM H_2O_2; therefore, these data points were used to generate Figure 5 and to determine the molar extinction coefficient of compound 5 at 590 nm under our assay conditions to be 6.6×10^4 M^{-1} cm^{-1}, as discussed in the caption of Figure 3.

Table 1. Comparison of assay performance in sodium phosphate and potassium phosphate buffers.

100 mM NaPi pH 6.5, Abs at 590 nm				100 mM KPi pH 7.6, Abs at 590 nm			
5 min		30 min		5 min		30 min	
NPC	Reaction	NPC	Reaction	NPC	Reaction	NPC	Reaction
0.17	0.84	0.50	3.6	0.08	1.03	0.2	3.4
0.13	0.86	0.51	3.6	0.12	0.83	0.22	3.3
0.13	0.90	0.56	3.5	0.11	0.90	0.19	3.3

Conditions: 100 mM sodium phosphate buffer (pH 6.5) or 100 mM potassium phosphate buffer (pH 7.6), AAP (3 mM), CTA (15 mM), H_2O_2 (10 mM), (*S*)-2-heptylamine (5 mM), and HRP (10 μg mL^{-1}). Absorbance was measured at 590 nm after 5 and 30 min.

Table 2. Investigation of the assay's sensitivity at varied concentrations of H_2O_2.

[H_2O_2] / mM	Abs 590 nm
0.0	0.15
0.1	0.35
0.2	0.86
0.3	1.30
0.4	1.70
0.5	2.13
1	3.35
2	3.4
3	3.4
4	3.4
5	3.4

Conditions: 100 mM potassium phosphate buffer pH 7.6, AAP (3 mM), CTA (15 mM), varied H_2O_2 concentrations (0–5 mM), and HRP (10 μg mL^{-1}). Absorbance was measured at 590 nm after 5 min.

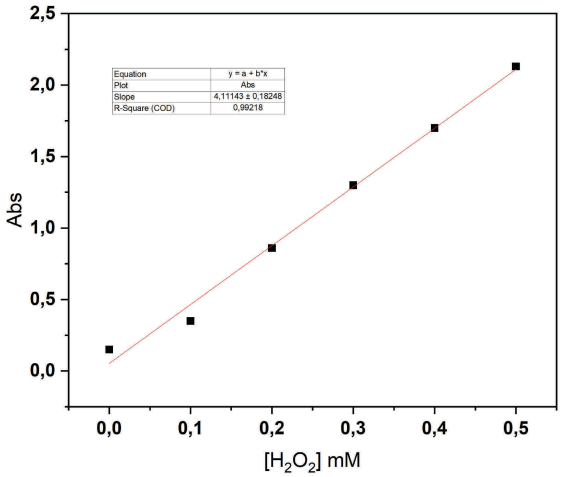

Figure 5. Linear correlation (R^2 = 0.992) between absorbance at 590 nm and H_2O_2 concentration in the CTA/AAP-HRP assay. The molar extinction coefficient of compound 5 was calculated from the slope of the linear fit (4111 M^{-1}) and the optical path length according to the Beer–Lambert law.

While all results with CTA were obtained using externally added H_2O_2, the next step was to assess whether H_2O_2 generated in situ by MAO-D5 could be used for detection. Reactions were prepared using crude MAO-D5 lysate (15 μL) and varying concentrations of (*S*)-2-heptylamine (7), but no color formation was observed. This suggested that CTA may inhibit MAO activity.

To investigate this possibility, we turned to an alternative assay based on 2,4,6–tribromo–3–hydroxybenzoic acid (TBHBA), which could offer a less inhibitory detection system (Figure 3a). As a positive control, reactions were performed using 5 mM (*S*)-*α*-methylbenzylamine (8) in the presence of TBHBA (1) and 4–aminoantipyrine (2). When combined with MAO-D5 cell-free extract (5–15 μL), a strong magenta color appeared within 10 minutes, confirming enzyme activity. In contrast, the test assay with (*R*)-enantiomer resulted in no coloration even after 24 hours, demonstrating the high enantioselectivity of MAO-D5. Furthermore, non-protein controls lacking MAO-D5 remained colorless, confirming that color development depended entirely on enzymatic H_2O_2 formation.

Having confirmed MAO-D5 activity under these assay conditions, we reconsidered whether the lack of signal in the CTA-based assay was due not to CTA-mediated inhibition, but rather to poor substrate recognition of (*S*)-2-heptylamine (7) by MAO-D5. To test this, we evaluated racemic 2-hexylamine under the same TBHBA-based assay conditions. A magenta signal became visible within 20 minutes for substrate concentrations between 0.5–5 mM, while reactions with 0.1 mM required approximately 3 hours for detectable coloration. These results confirmed that MAO-D5 efficiently accepts 2-hexylamine and that the assay is sensitive to low H_2O_2 concentrations. Based on these findings, we concluded that CTA likely inhibits MAO-D5 and therefore proceeded with further experiments using the TBHBA-based assay system.

Having established that the TBHBA-based assay reliably reports MAO-D5 activity in the presence of (*S*)-configured amines and demonstrates both high sensitivity and enantioselectivity, we next integrated it into the final high-throughput screening protocol for engineered D-AADH variants. The goal was to directly detect the formation of (*S*)-configured amines via reductive amination, using H_2O_2 generation as a selective and quantifiable signal. With this setup, MAO-D5 acts as a stereochemical gatekeeper accepting only (*S*)-amines and producing H_2O_2 stoichiometrically, which is subsequently detected via the colorimetric HRP cascade. Under the assay conditions, we expect that the intensity of the colorimetric signal will reflect the relative amount of the oxidizable (*S*)-configured amine, and therefore may correlate with the enantiomeric composition of the reaction mixture to a certain extent. The finalized protocol consists of two sequential steps following enzyme purification. First, 50 μL of the reaction mixture (RM) were added to 50 μL of the purified AmDH. The RM contained ketone (10 mM), glucose dehydrogenase (GDH, 2 mg mL^{-1}), D-glucose (100 mM), and NADP$^+$ (2 mM) in 400 mM NH_4Cl buffer (pH 9), supplemented with 100 mM K_2CO_3, conditions optimized for this enzyme.[42,45] After the reductive amination step, 200 μL of the assay solution (AS) was added, consisting of 0.54 mM of compound 1, 0.75 mM of compound 2, 15 μL MAO-D5 crude cell lysate, and 10 μg mL^{-1} HRP in 500 mM KPi buffer (pH 7.6).

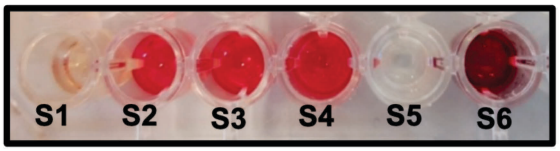

Figure 6. Colorimetric assay for the detection of amine formation under simulated screening conditions. The reactions (S2-S4) consist of 5 mM 2-hexanone and 5 mM 2-hexylamine with elution buffer containing D-AADH (1 mg mL^{-1}). This mixture was then combined with assay solution containing TBHBA (0.54 mM), AAP (0.75 mM), MAO-D5 crude cell lysate (15 µL), and HRP (10 µg mL^{-1}) in KPi buffer (500 mM, pH 7.6).

To simulate a hypothetical scenario of 50 % conversion of 10 mM 2-hexanone to the corresponding amine compound, a mock reaction was prepared containing 5 mM 2-hexanone and 5 mM 2-hexylamine. This was mixed with elution buffer containing 1 mg mL^{-1} D-AADH and subsequently combined with the assay solution. The reaction was performed in triplicate (S2–S4), with negative control lacking amine (S1) or containing only ketone (S5) and one positive control (S6) containing 5 mM 2-hexylamine directly in the AS without any RM or D-AADH (Figure 6).

After 24 hours, all test reactions (S2–S4) developed a clear magenta color, while the negative controls (S1) or (S5) remained uncolored. The positive control without ketone (S6) yielded the expected coloration, confirming the assay's functionality.

Assessment of Throughput and Sensitivity in a Directed Evolution Campaign

To evaluate the practical applicability of the developed *ee*-HTS assay under realistic enzyme engineering conditions, the final protocol was applied in a directed evolution campaign involving the screening of a library of D-AADH variants (Figure 7). Approximately 7,400 variants distributed across 77 microtiter plates were screened using the sequential two-step protocol consisting of: (i) reductive amination

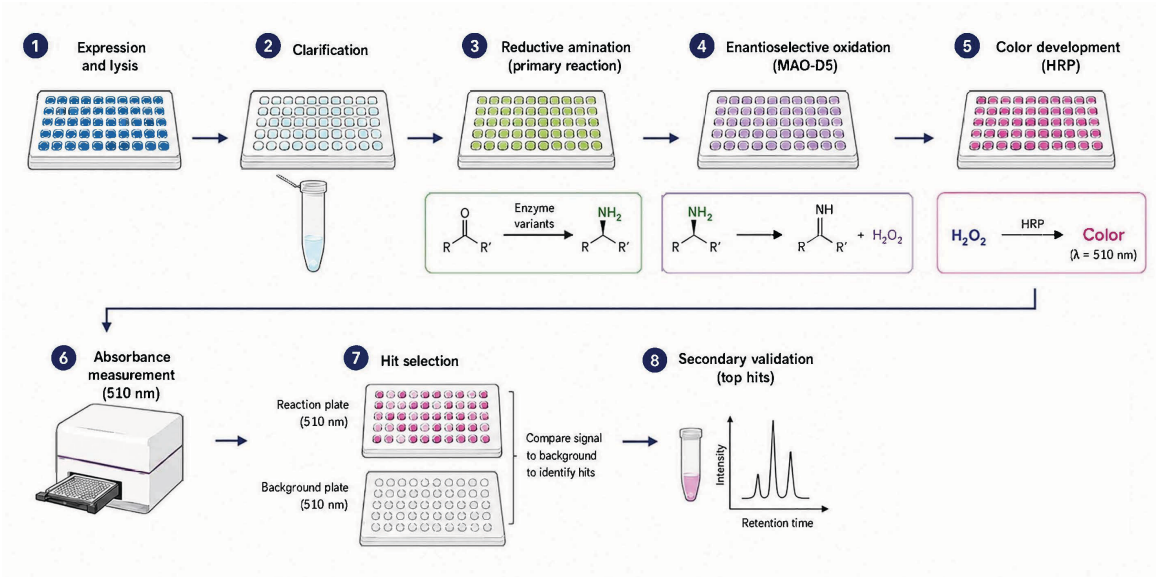

Figure 7. Schematic overview of the workflow used to screen D-AADH variants in 96-well plate format. Step 1: D-AADH variant libraries are expressed in microplate format, and cells are lysed to obtain enzyme-containing crude lysates. Step 2: Lysates are transferred to paired reaction and background-control plates. Step 3: The enzymatic reaction is performed by adding the reaction mixture (RM) to the enzyme-containing lysate. The RM contains ketone substrate (10 mM), glucose dehydrogenase (GDH, 2 mg mL^{-1}), D-glucose (100 mM), $NADP^+$ (2 mM), NH_4Cl buffer (400 mM, pH 9), and K_2CO_3 (100 mM). This first step enables reductive amination and potential formation of the target chiral amine. Step 4–5: MAO-D5 selectively oxidizes the formed (*S*)-configured amine to the corresponding imine, generating H_2O_2 as a stoichiometric by-product. The assay solution contains MAO-D5 crude cell lysate, horseradish peroxidase (HRP, 10–20 µg mL^{-1}), 4-aminoantipyrine (AAP, 0.75 mM), and 2,4,6-tribromo-3-hydroxybenzoic acid (TBHBA, 0.54 mM) in potassium phosphate buffer (KPi, 500 mM, pH 7.6). H_2O_2 is detected through HRP-mediated coupling, resulting in the formation of a magenta-colored product. Step 6: Reaction plates are compared directly with the corresponding background plates lacking substrate, and variants are ranked based on the absorbance difference at 510 nm. Step 7: Variants showing the highest signal-to-background differences are selected for secondary validation by GC analysis at Step 8.

catalyzed by the D-AADH variants and (ii) stereoselective oxidation of the generated amine product by MAO-D5 coupled with HRP-mediated color formation. The screening campaign was performed in an aqueous 96-well plate format using crude lysates, with absorbance measured at 510 nm. The assay enabled rapid ranking of variants based on the measured absorbance values relative to the corresponding backgrounds (i.e., negative controls).

Approximately 200 variants that produced the highest colorimetric responses were selected for secondary analysis, re-expressed and purified on a small scale, and subsequently evaluated by GC-FID following biocatalytic reactions. This initial D-AADH library did not ultimately contain variants capable of converting the selected substrate at synthetically useful levels. We detected only trace formation (< 1 % conversion) of the target amine, most likely due to the highly challenging nature of the enzyme engineering project, and/or the too low size and diversity of the D-AADH library. Nevertheless, we were able to demonstrate that the assay itself functions effectively, as even trace product formation could be detected. Importantly, the results also highlight the role of the colorimetric assay as a primary screening tool for potential hit identification and ranking, while confirming the need for secondary analytical validation by GC or HPLC to quantify product formation and exclude false-positive hits. Therefore, the assay is intended primarily as a high-throughput qualitative to semi-quantitative screening method rather than as a precise method for the quantitative determination of AmDH activity.

Importantly, the screening of the D-AADH variant library also provided insight into the balance between assay sensitivity and throughput. Under the optimized protocol, 1.5 h of color development at 30 °C was sufficient for same-day variant ranking by absorbance measurement at 510 nm. Approximately 7400 D-AADH variants were screened across 77–79 plates. With manual handling of approximately four plates per day, a library of this size can

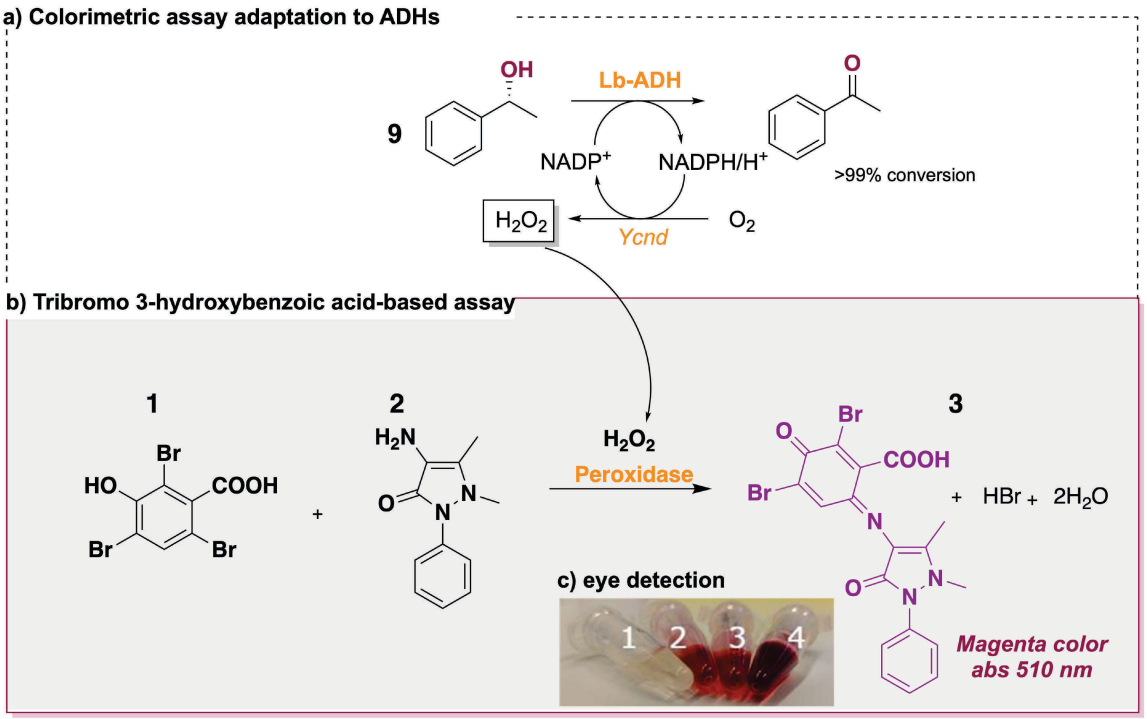

Figure 8. Generalization of the TBHBA/AAP–HRP colorimetric assay to alcohol dehydrogenase activity. (a) Schematic representation of the coupled assay, in which Lb-ADH catalyzes the oxidation of (*R*)-1-phenylethanol to acetophenone with concomitant reduction of $NADP^+$ to NADPH. YcnD then reoxidizes NADPH to $NADP^+$ using molecular oxygen, generating H_2O_2, which is detected by HRP-mediated oxidation of TBHBA/AAP to form a magenta-colored product. (b) Representative colorimetric assay. The reaction mixture contained Lb-ADH (45 μM), YcnD (10 μM), $NADP^+$ (0.5 mM), HRP (20 μg mL^{-1}), (*R*)-1-phenylethanol (20 mM), TBHBA (5.4 mM), and AAP (7.5 mM) in buffer. (c) Eye-detection image of the Lb-ADH/YcnD-coupled colorimetric assay; sample 1 is the non-protein control lacking Lb-ADH; samples 2 and 3 are reactions containing Lb-ADH and independent YcnD preparations; sample 4 is a positive control containing externally added H_2O_2 (10 mM). Magenta coloration indicates H_2O_2 formation coupled to alcohol oxidation.

be screened in about 20 working days, demonstrating the practical suitability of the assay for early-stage directed evolution campaigns. Admittedly, the method now needs to be applied to the screening of larger and more diverse variant libraries, possessing significantly higher catalytic activities.

Generalization of the Colorimetric Assay for Diverse Oxidoreductase Activities

Beyond its use with the enantioselective synthesis of chiral amines for NAD(P)H-dependent oxidoreductases like AmDHs or reductive aminases (RedAms), this colorimetric platform can be generalized to other oxidoreductases, such as alcohol dehydrogenases (ADHs), demonstrating its versatility for broader biocatalyst screening. As proof of concept, the assay was adapted into a simplified two-enzyme cascade. In the first oxidative step, the ADH catalyzes the stereoselective oxidation of an enantiopure alcohol to its corresponding ketone or aldehyde, reducing $NADP^+$ to NADPH. To regenerate $NADP^+$ and couple the assay to color development, the highly specific NADPH oxidase YcnD from *Bacillus subtilis* was employed.[46] YcnD oxidizes NADPH back to $NADP^+$ using molecular oxygen and generates stoichiometric hydrogen peroxide (H_2O_2) as a byproduct.[47] The in situ formation of H_2O_2 is subsequently detected via the peroxidase-based chromogenic reaction (Figure 8). Thus, this system enables direct evaluation of ADH activity and enantioselectivity through a colorimetric readout.

As mentioned, H_2O_2 generated by YcnD-catalyzed O_2 reduction is coupled to horseradish-peroxidase-mediated dye formation, utilizing 2,4,6-tribromo-3-hydroxybenzoic acid and 4-aminoantipyrine as substrates (Figure 8). To evaluate the ADH assay, we selected the anti-Prelog, NADP-dependent ADH from *Lactobacillus brevis* (Lb-ADH) as a model enzyme. Lb-ADH is a well-characterized enzyme with extensive literature describing its substrate scope and stereoselectivity, making it an ideal benchmark candidate for validating the generality of the platform.[39,48,49]

After successfully expressing and purifying Lb-ADH and YcnD, the assay mixture contained Lb-ADH (45 µM), YcnD (10 µM), $NADP^+$ (0.5 mM), HRP (20 µg mL^{-1}), and 1-phenylethanol (20 mM) as substrate. In this reaction, Lb-ADH catalyzes the enantioselective oxidation of (*R*)-1-phenylethanol (9) to acetophenone, thus enabling direct correlation between color formation and enzyme enantioselectivity. Reactions containing both Lb-ADH and YcnD developed a distinct magenta coloration within hours (Figure 8c, samples 2–3), whereas the non-protein control (NPC, Figure 8c, sample 1) remained colorless. A positive control with externally added H_2O_2 (10 mM) was also included in the experiment (Figure 8c, sample 4). These visual results were corroborated by GC-FID analysis, which confirmed > 99 % substrate conversion. This dual validation underscores the assay's sensitivity, reliability, and versatility for high-throughput screening of different dehydrogenases.

CONCLUSIONS

In this study, we have developed a robust, enantioselective high-throughput screening platform that integrates efficient expression and purification of oxidoreductases in a 96-well plate format with a colorimetric readout based on hydrogen peroxide detection. Using MAO-D5 as a stereoselective gatekeeper, the assay reliably distinguishes (*S*)-amines from their (*R*)-counterparts and converts enantiomer recognition into a colorimetric signal. The TBHBA/AAP–HRP cascade demonstrated high sensitivity, low background, and clear discrimination in both mock and enzymatic reactions, validating its suitability for screening engineered amine dehydrogenase libraries. The applicability of the present assay is dependent on the selectivity and substrate scope of the reporter oxidase used for stereochemical discrimination. In this study, MAO-D5 enables selective detection of (*S*)-configured amines; however, the degree of enantiomeric discrimination can be substrate-dependent and, therefore, this feature has to be determined on a case-by-case basis before starting the screening of variants toward a specific substrate. In addition, the limited availability of complementary (*R*)-selective oxidases currently restricts broader application toward both enantiomeric series. Furthermore, successful implementation of the assay requires overlapping substrate compatibility between the reporter oxidase and the target oxidoreductase. Despite these limitations, the assay provides a simple and accessible platform for rapid enantioselective screening in aqueous microplate formats without the need for derivatization or specialized instrumentation. Importantly, we showed that this principle extends beyond amine synthesis. By coupling alcohol dehydrogenase activity to NADPH re-oxidation catalyzed by YcnD, we established a generalizable two-enzyme cascade that produces stoichiometric hydrogen peroxide, enabling enantioselective detection of alcohols. Application to *Lactobacillus brevis* ADH confirmed both activity and stereoselectivity, with visual results fully supported by GC-FID analysis. Collectively, these results demonstrate that the platform is sensitive, scalable, and adaptable across dehydrogenase enzyme families. By directly linking enantiomer recognition to a simple colorimetric readout, this system addresses the need for rapid and selective identification of stereoselective variants while minimizing reliance on derivatization, specialized equipment, or low-throughput analytics. Future work will focus on applying this assay to large-scale mutagenesis campaigns, thereby accelerating the discovery and optimization of novel stereoselective biocatalysts for sustainable synthesis.

Acknowledgment. F.G.M. thanks the Dutch Research Council (NWO) for an NWO XS grant (No: OCENW.XS24.3.183), and the EU Horizon Europe Marie Skłodowska-Curie Actions (MSCA) for the YcascadE (No: 101153173) and SuBStrAte (No: 101208425) grants. V.T. thanks NWO for Veni grant VI.Veni.232.268.

REFERENCES

[1] N. Nyangchak, *J. Clean. Prod.* **2022**, *378*, 134622, https://doi.org/10.1016/j.jclepro.2022.134622.

[2] J. Colberg, K. Kuok Hii, S. G. Koenig, *Org. Process Res. Dev.* **2022**, *26*, 2176–2178. https://doi.org/10.1021/acs.oprd.2c00171.

[3] R. Sánchez Morales, P. Sáenz-López, M. A. de las Heras Perez, *Sustainability* **2024**, *16*, 6526. https://doi.org/10.3390/su16156526.

[4] M. M. Musa, F. Hollmann, F. G. Mutti, *Catal. Sci. Technol.* **2019**, *9*, 5487–5503. https://doi.org/10.1039/C9CY01539F.

[5] R. U. McVicker, N. M. O'Boyle, *J. Med. Chem.* **2024**, *67*, 2305–2320. https://doi.org/10.1021/acs.jmedchem.3c02239.

[6] V. Tseliou, M. F. Masman, T. Knaus, F. G. Mutti, *ChemCatChem* **2024**, *16*, e202400469. https://doi.org/10.1002/cctc.202400469.

[7] G. A. Aleku, *ACS Catal.* **2024**, *14*, 14308–14329. https://doi.org/10.1021/acscatal.4c04756.

[8] R. Kumar, M. J. Karmilowicz, D. Burke, M. P. Burns, L. A. Clark, C. G. Connor, E. Cordi, N. M. Do, K. M. Doyle, S. Hoagland, C. A. Lewis, D. Mangan, C. A. Martinez, E. L. McInturff, K. Meldrum, R. Pearson, J. Steflik, A. Rane, J. Weaver, *Nat. Catal.* **2021**, *4*, 775–782. https://doi.org/10.1038/s41929-021-00671-5.

[9] M. Schober, C. MacDermaid, A. A. Ollis, S. Chang, D. Khan, J. Hosford, J. Latham, L. A. F. Ihnken, M. J. B. Brown, D. Fuerst, M. J. Sanganee, G.-D. Roiban, *Nat. Catal.* **2019**, *2*, 909–915. https://doi.org/10.1038/s41929-019-0341-4.

[10] E. J. Ma, E. Siirola, C. Moore, A. Kummer, M. Stoeckli, M. Faller, C. Bouquet, F. Eggimann, M. Ligibel, D. Huynh, G. Cutler, L. Siegrist, R. A. Lewis, A.-C. Acker, E. Freund, E. Koch, M. Vogel, H. Schlingensiepen, E. J. Oakeley, R. Snajdrova, *ACS Catal.* **2021**, *11*, 12433–12445. https://doi.org/10.1021/acscatal.1c02786.

[11] J. Steflik, A. Gilio, M. Burns, G. Grogan, R. Kumar, R. Lewis, C. Martinez, *ACS Catal.* **2023**, *13*, 10065–10075. https://doi.org/10.1021/acscatal.3c01534.

[12] R. Buller, S. Lutz, R. J. Kazlauskas, R. Snajdrova, J. C. Moore, U. T. Bornscheuer, *Science* **2023**, *382*, eadh8615. https://doi.org/10.1126/science.adh8615.

[13] A. O'Connell, A. Barry, A. J. Burke, A. E. Hutton, E. L. Bell, A. P. Green, E. O'Reilly, *Chem. Soc. Rev.* **2024**, *53*, 2828–2850. https://doi.org/10.1039/D3CS00689A.

[14] M. T. Reetz, A. Zonta, K. Schimossek, K. E. Jaeger, K. Liebeton, *Angew. Chem. Int. Ed.* **2004**, *36*, 2830–2832. https://doi.org/10.1002/anie.199728301.

[15] P. Abato, C. T. Seto, *J. Am. Chem. Soc.* **2001**, *123*, 9206–9207. https://doi.org/10.1021/ja016177q.

[16] G. A. Korbel, G. Lalic, M. D. Shair, *J. Am. Chem. Soc.* **2001**, *123*, 361–362. https://doi.org/10.1021/ja0034747.

[17] M. T. Reetz, K. M. Kühling, S. Wilensek, H. Husmann, U. W. Häusig, M. Hermes, *Catal. Today* **2001**, *67*, 389–396. https://doi.org/10.1016/S0920-5861(01)00331-5.

[18] M. T. Reetz, F. Daligault, B. Brunner, H. Hinrichs, A. Deege, *Angew. Chem. Int. Ed.* **2004**, *43*, 4078–4081. https://doi.org/10.1002/anie.200460311.

[19] W. Schrader, A. Eipper, D. J. Pugh, M. T. Reetz, *Can. J. Chem.* **2002**, *80*, 626–632. https://doi.org/10.1139/v02-069.

[20] F. Cedrone, S. Niel, S. Roca, T. Bhatnagar, N. Ait-abdelkader, C. Torre, H. Krumm, A. Maichele, M. T. Reetz, J. C. Baratti, *Biocatal. Biotransform.* **2003**, *21*, 357–364. https://doi.org/10.1080/102420310001630137.

[21] G. DeSantis, K. Wong, B. Farwell, K. Chatman, Z. Zhu, G. Tomlinson, H. Huang, X. Tan, L. Bibbs, P. Chen, K. Kretz, M. J. Burk, *J. Am. Chem. Soc.* **2003**, *125*, 11476–11477. https://doi.org/10.1021/ja035742h.

[22] M. T. Reetz, A. Eipper, P. Tielmann, R. Mynott, *Adv. Synth. Catal.* **2002**, *344*, 1008–1016. https://doi.org/10.1002/1615-4169(200210)344:9<1008::AID-ADSC1008>3.0.CO;2-T

[23] P. Tielmann, M. Boese, M. Luft, M. T. Reetz, *Chem. Eur. J.* **2003**, *9*, 3882–3887. https://doi.org/10.1002/chem.200304885.

[24] M. T. Reetz, K. M. Kühling, A. Deege, H. Hinrichs, D. Belder, *Angew. Chem. Int. Ed.* **2000**, *39*, 3891–3893. https://doi.org/10.1002/1521-3773(20001103)39:21<3891::AID-ANIE3891>3.0.CO;2-1

[25] M. T. Reetz, K. M. Kühling, H. Hinrichs, A. Deege, *Chirality* **2000**, *12*, 479–482. https://doi.org/10.1002/(SICI)1520-636X(2000)12:5/6<479::AID-CHIR32>3.0.CO;2-#

[26] M. Gantz, S. V. Mathis, F. E. H. Nintzel, M. Penner, P. J. Zurek, T. Knaus, V. Tseliou, E. Patel, D. Boros, F.-M. Weberling, M. R. A. Kenneth, O. J. Klein, E. J. Medcalf, J. Moss, M. Herger, T. S. Kaminski, F. G. Mutti, P. Lio, F. Hollfelder, *bioRxiv* **2025**, 2024.2004.2008.588565. https://doi.org/10.1101/2024.04.08.588565.

[27] S. Chen, P. C. Engel, *J. Biotechnol.* **2009**, *142*, 127–134. https://doi.org/10.1016/j.jbiotec.2009.03.005.

[28] J. R. Marshall, P. Yao, S. L. Montgomery, J. D. Finnigan, T. W. Thorpe, R. B. Palmer, J. Mangas-Sanchez, R. A. M. Duncan, R. S. Heath, K. M. Graham, D. J. Cook, S. J. Charnock, N. J. Turner, *Nat. Chem.* **2021**, *13*, 140–148. https://doi.org/10.1038/s41557-020-00606-w.

[29] M. J. Abrahamson, E. Vázquez-Figueroa, N. B. Woodall, J. C. Moore, A. S. Bommarius, *Angew. Chem. Int. Ed.* **2012**, *51*, 3969–3972. https://doi.org/10.1002/anie.201107813.

[30] A. Pushpanath, E. Siirola, A. Bornadel, D. Woodlock, U. Schell, *ACS Catal.* **2017**, *7*, 3204–3209. https://doi.org/10.1021/acscatal.7b00516.

[31] T. Ghosh, J. Sicheri, D. H. Kwan, *bioRxiv* **2025,** 2025.06.15.659766. https://doi.org/10.1101/2025.06.15.659766.

[32] G. Y. Yang, A. M. Shamsuddin, *Histol. Histopathol.* **1996**, *11*, 801–806. https://pubmed.ncbi.nlm.nih.gov/8839767/.

[33] P. D. Josephy, T. Eling, R. P. Mason, *J. Biol. Chem.* **1982**, *257*, 3669–3675. https://doi.org/10.1016/S0021-9258(18)34832-4.

[34] M. Gabler, M. Hensel, L. Fischer, *Enzyme Microb. Technol.* **2000**, *27*, 605–611. https://doi.org/10.1016/S0141-0229(00)00262-3.

[35] J. Xing, G. Orderley, R. T. Bradshaw Allen, N. N. Ahmad, C. Gourjault, A. Akgul, S. O. Alhassan, N. Ngernanek, S. Salke, G. A. Aleku, *JACS Au* **2025**, *5*, 3468–3482. https://doi.org/10.1021/jacsau.5c00512.

[36] H. Joo, A. Arisawa, Z. Lin, F. H. Arnold, *Chemistry & Biology* **1999**, *6*, 699–706. https://doi.org/10.1016/S1074-5521(00)80017-4.

[37] Y. Shao, Y.-D. Gao, Z.-L. He, L.-C. Yang, *Chem Catal.* **2024**, *4*, 101068. https://doi.org/10.1016/j.checat.2024.101068.

[38] D. J. Bougioukou, S. Kille, A. Taglieber, M. T. Reetz, *Adv. Synth. Catal.* **2009**, *351*, 3287–3305. https://doi.org/10.1002/adsc.200900644.

[39] M. Damian, F. G. Mutti, *Eur. J. Org. Chem.* **2023**, *26*, e202300734. https://doi.org/10.1002/ejoc.202300734.

[40] B. R. Bommarius, M. Schürmann, A. S. Bommarius, *Chem. Commun.* **2014**, *50*, 14953–14955. https://doi.org/10.1039/C4CC06527A.

[41] T. Knaus, W. Böhmer, F. G. Mutti, *Green Chem.* **2017**, *19*, 453–463. https://doi.org/10.1039/C6GC01987K.

[42] K. Vedha-Peters, M. Gunawardana, J. D. Rozzell, S. J. Novick, *J. Am. Chem. Soc.* **2006**, *128*, 10923–10929. https://doi.org/10.1021/ja0603960.

[43] V. F. Batista, J. L. Galman, D. C. G. A. Pinto, A. M. S. Silva, N. J. Turner, *ACS Catal.* **2018**, *8*, 11889–11907. https://doi.org/10.1021/acscatal.8b03525.

[44] C. J. Dunsmore, R. Carr, T. Fleming, N. J. Turner, *J. Am. Chem. Soc.* **2006**, *128*, 2224–2225. https://doi.org/10.1021/ja058536d.

[45] F. Parmeggiani, S. T. Ahmed, M. P. Thompson, N. J. Weise, J. L. Galman, D. Gahloth, M. S. Dunstan, D. Leys, N. J. Turner, *Adv. Synth. Catal.* **2016**, *358*, 3298–3306. https://doi.org/10.1002/adsc.201600682.

[46] A. Morokutti, A. Lyskowski, S. Sollner, E. Pointner, T. B. Fitzpatrick, C. Kratky, K. Gruber, P. Macheroux, *Biochemistry* **2005**, *44*, 13724–13733. https://doi.org/10.1021/bi0510835.

[47] T. Knaus, L. Cariati, M. F. Masman, F. G. Mutti, *Org. Biomol. Chem.* **2017**, *15*, 8313–8325. https://doi.org/10.1039/C7OB01927K.

[48] F. G. Mutti, T. Knaus, N. S. Scrutton, M. Breuer, N. J. Turner, *Science* **2015**, *349*, 1525–1529. https://doi.org/10.1126/science.aac9283.

[49] K. Niefind, J. Muller, B. Riebel, W. Hummel, D. Schomburg, *J. Mol. Biol.* **2003**, *327*, 317–328. https://doi.org/10.1016/S0022-2836(03)00081-0.